ACS APPLIED MATERIALS & INTERFACES

Research Article

www.acsami.org

Activatable Ferritin Nanocomplex for Real-Time Monitoring of Caspase-3 Activation during Photodynamic Therapy

Jingjing Wang,[†] Liwen Zhang,[†] Minglong Chen,[‡] Shi Gao,*[,‡] and Lei Zhu*[,†]

[†]State Key Laboratory of Molecular Vaccinology and Molecular Diagnostics & Center for Molecular Imaging and Translational Medicine, School of Public Health, Xiamen University, Xiamen 361005, China

[‡]China-Japan Union Hospital, Jilin University, Changchun 130033, China

Supporting Information

ABSTRACT: One mechanism of photodynamic therapy (PDT) for the ablation of tumors is to induce apoptosis. Visualization of apoptosis during PDT in real-time is of great benefit for predicting and evaluating therapeutic outcomes. Herein, we engineered a highly stable and sensitive caspase-3 ferritin activatable probe (FABP/ZnPc) for simultaneous delivery of a photosensitizer (ZnPc) and real-time visualization of apoptosis during PDT. Upon near-infrared (NIR) light irradiation, ZnPc becomes active and initiates apoptosis, upon which the outer layer of the FABP/ZnPc is degraded by the apoptotic marker, caspase-3, to boost strong fluorescent signals, ultimately allowing real-time imaging of apoptosis. Our results demonstrate the utility of FABP/ZnPc as a tool for PDT and simultaneous imaging of caspase-3 activation in vitro and in vivo. Overall, the ability of FABP/ZnPc to image apoptosis during PDT will not only facilitate optimizing and personalizing the PDT strategy but is also important for understanding the mechanisms of PDT.

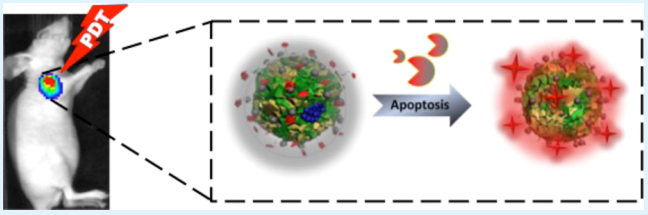

KEYWORDS: *photodynamic therapy, apoptosis, caspase-3, activatable probe, ferritin*

INTRODUCTION

Photodynamic therapy (PDT) is clinically approved for the treatment of various diseases, including cancers.[1,2] Theoretically, PDT utilizes thermoneutral light of specific wavelengths to excite nontoxic photosensitizers to produce toxic reactive oxygen species (ROS) and/or singlet oxygen ($^1O_2$), leading to selective tissue destruction and vascular damage.[1,3] The advantages of PDT over other conventional cancer treatments are the superiority of noninvasive, low systemic toxicity and therefore minimal side effects.[4,5] Notably, PDT is an alternative treatment strategy for those suffering from chemo/radio resistance because it kills cancer cells through another pathway. One of the most possible mechanisms of PDT for tumors is to induce apoptosis by generating ROS and/or $^1O_2$.[6,7] Direct and simultaneous visualization of apoptosis during PDT will help (i) investigate the relationship between PDT cytotoxicity and cellular changes; (ii) elucidate the complex mechanism of PDT of diseases; (iii) predict and evaluate therapeutic effects,[8] especially for those suffering from chemo/radio resistance;[9] and (iv) facilitate the photosensitizer screening and optimization.[9−12]

Many studies have reported that apoptosis is initiated during PDT,[13−16] but few of those works clarify the details of apoptosis during the therapy. To date, the gold standard approach to confirm apoptosis is using dye-labeled Annexin V for recognition of phosphatidylserine (PS) on the apoptotic cell membrane. Although simple, the method is indirect and is not completely specific to apoptosis.[17] Alternatively, a family of cysteine dependent aspartate-directed proteases (caspases) has attracted great interest in apoptosis imaging, because these proteinases are closely relevant and crucial mediators/effectors to apoptosis.[18−22] A number of innovative methods have been developed to image caspase expression in live cells.[12] Among them, fluorescence resonance energy transfer (FRET) based fluorogenic probes, which are composed of a peptide backbone conjugated with a FRET pair, are promising agents in apoptosis imaging due to their improved target-to-background ratio, sensitivity, and specificity.[23−28] Particularly, we previously reported real-time imaging of caspase-8 and caspase-3 cascade activation with a peptide transfection agent.[12] In addition, a multicolor activatable nanocomplex was also developed for simultaneous visualization of caspase-8/9/3 activation.[29] Such FRET-based activatable probes targeting caspases for apoptosis imaging are reported elsewhere as well.[26,30,31] Additionally, engineered fluorescent and luminescent proteins are also developed for caspase-mediated apoptosis imaging.[31−34] These strategies always require tedious steps to visualize the caspase activation process, for example, adding exogenous apoptosis inducers or using genetically engineered cells. Although some fluorescent photosensitizer conjugates are able to simultaneously provide static caspase imaging during PDT,[35−37] the sensitivity and *in vivo* applications of these photosensitizer based probes are a concern due to the low photostability and structural stability of fluorescent photo-

Received: August 11, 2015
Accepted: September 21, 2015
Published: September 21, 2015

DOI: 10.1021/acsami.5b07316
ACS Appl. Mater. Interfaces 2015, 7, 23248−23256

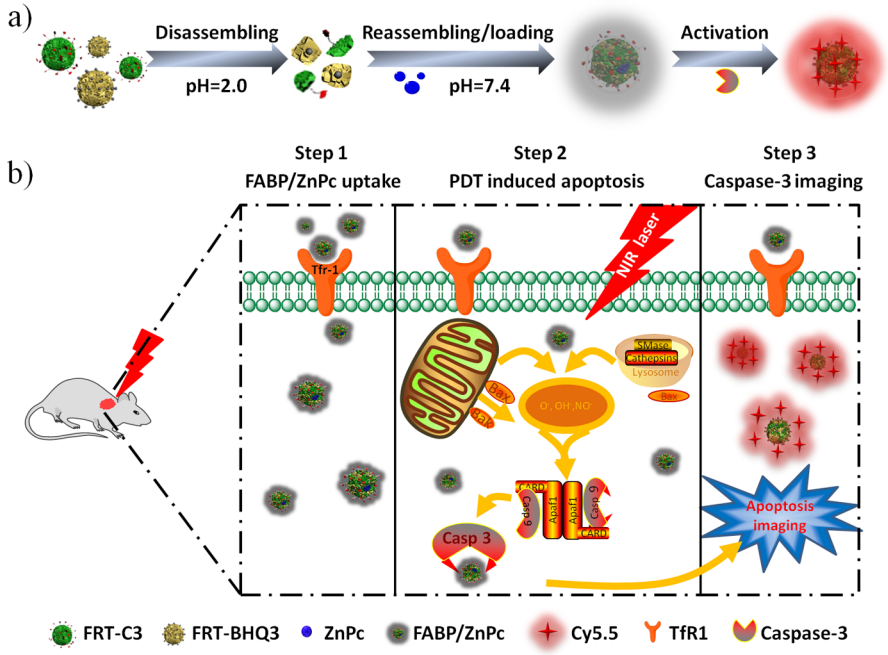

Figure 1. Design and preparation of FABP/ZnPc: (a) compositions and constructions of FABP/ZnPc and (b) schematic presentation of the molecular mechanism of intracellular FABP/ZnPc for real-time monitoring of caspases-3 activation during photodynamic therapy (PDT).

sensitizer.[38,39] Moreover, complex synthetic steps are always required for a limited number of photosensitizers to construct such linear peptide probes that requires the photosensitizers to be fluorescent and easy to be modified. Given these considerations, development of a facile, stable, and sensitive apoptosis imaging agent during PDT with high signal-to-background ratio is highly desirable.

Herein, we present a novel nanocomplex that enable effective PDT of MDA-MB-435 tumors and provide real-time imaging of caspase-3 activation (Figure 1). The complex is based on a biocompatible ferritin nanoparticle (FRT), a major iron storage protein composed of 24 subunits of L- and H-chains with varied proportion. FRT subunits can self-assemble into a cage-like structure at neutral conditions and disassemble at acidic conditions. Both ferritin surface and inner cage are ideal for modification with different agents depending on the purposes of constructing this complex. Importantly, FRT will cause less clinical concerns than traditional synthetic carriers as a natural existing polymer. We have previously reported that successfully utilizing FRT based probe for imaging extracellular proteinase in a tumor bearing mouse model,[40] and in this work the applications of FRT were designed to investigate intracellular apoptosis related proteinase during PDT. Specifically, FRT was modified with NIR dye labeled caspase-3 specific substrates (Figure S1) and black hole quencher-3 (BHQ3) (Figure S2) on the outer layer and denoted as FABP. A metal-chelated photosensitizer, zinc(II) phthalocyanine (ZnPc), was embedded inside the nanosenor for a therapeutic role by simply mixing and named as FABP/ZnPc (Figure 1a). Upon NIR laser irradiation, the built-in photosensitizer ZnPc will be activated and generate ROS/$^1O_2$ to induce apoptosis. Then, the caspase-3 specific peptide substrate labeled on the outside of the FABP/ZnPc will be cleaved by activated caspase-3 and boost strong fluorescence signals in a time-dependent manner. Compared with the fluorescent photosensitizer conjugated linear peptide probes for apoptosis detection during PDT, the PDT-activatable FRT nanocomplex presented in this contribution holds multiple NIR dyes on a single particle with high photostability. It is therefore ideal for detecting of caspase-3 activation both in live cells and *in vivo* in real-time, which facilitates understanding of PDT-induced apoptosis mechanisms as well as predicting personalized treatment outcome (Figure 1b). Importantly, the ample encapsulated ZnPc (>60%, w/w) in FABP can be simply replaced with other kind of photosensitizer by mixing, allowing a broad option of photosensitizer for evaluations.

MATERIALS AND METHODS

Preparation of Hybrid Ferritins. For Cy5.5-tagged peptide coupling, *N*-succinimidyl-4-maleimidobutyrate (800 nmol in 10 μL DMSO) was added into a ferritin solution in PBS (50 nmol, 500 μL). The mixture was incubated in a 1.5 mL eppendorf tube at room temperature for 1 h with gentle shaking with a pH of 7.4. The conjugated ferritin was purified by NAP-5 column pre-equilibrated with PBS buffer and concentrated to 0.5 mL by the YM-10 centricon. Subsequently, a total of 80 nmol of Cy5.5-tagged peptide (NH2-Gly-Asp-Glu-Val-Asp-Ala-Pro-Cys-OH) in PBS was added into the conjugated ferritin solution, and the reaction proceeded at room temperature overnight with gentle shaking. The resulted FRT-C3 was purified by NAP-5 column pre-equilibrated with PBS buffer. For quencher conjugation, BHQ3 succinimide ester (400 nmol in 30 μL of DMSO) was added into the ferritin solution (50 nmol in 500 μL of PBS). The mixture was incubated in an eppendorf tube at room temperature for 1 h with gentle shaking. The resulting FRT-BHQ3 was purified by the NAP-5 column pre-equilibrated with PBS buffer.

Ferritin without iron inside, apoferritin, is used throughout in our study. To achieve the final hybrid ferritins (FABP/ZnPc), both types of ferritins were mixed and broken down to subunits by adjusting the pH to 2.0, and 100 μL of ZnPc (0.5 mg/mL) in DMSO was added with shaking. After 1 h, the pH was adjusted back to 7.4 with 1 M NaOH with gentle shaking. Free ZnPc was removed by NAP-5 column pre-equilibrated with PBS buffer and the solution was concentrated to 0.5 mL by the YM-10 centricon. The final product was named as FABP/ZnPc. The purity of FRT, FRT-C3, FRT-BHQ3, FABP, and FABP/ZnPc were confirmed by SDS-PAGE. The amount of Cy5.5 conjugated onto FRT was calculated according to the

DOI: 10.1021/acsami.5b07316
ACS Appl. Mater. Interfaces 2015, 7, 23248−23256

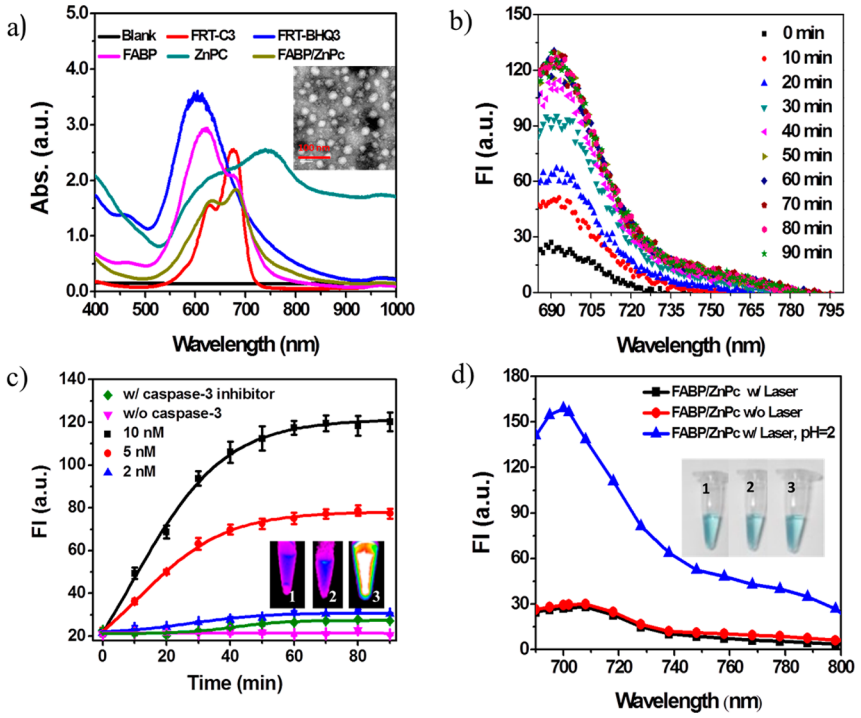

Figure 2. Characterizations of FABP/ZnPc: (a) NIR-UV−vis absorbance spectra of FRT-C3, FRT-BHQ3, ZnPc, FABP, and FABP/ZnPc. Insert: TEM images of FABP/ZnPc. Ex/em of Cy5.5, 675/695 nm. (b) Fluorescence intensity change over time of FABP/ZnPc (containing 0.45 μM of FRT-C3) with activated caspase-3. (c) Protease response of FABP (containing 0.45 μM of FRT-C3) in the presence of caspase-3 with different concentrations (0, 2, 5, 10 nM) and a caspase-3 inhibitor. Inner photos are fluorescence images of (1) FABP without caspase-3, (2) FABP with caspase-3 inhibitor, and (3) FABP with caspase-3. (d) Stability test of FABP/ZnPc (containing 20 μg/mL of ZnPc) under laser irradiation. In the chart are photos of (1) FABP/ZnPc without laser irradiation, (2) FABP/ZnPc with laser irradiation at 150 mW/cm^2 for 10 min, and (3) FABP/ZnPc w/o laser irradiation at pH = 2.

standard curve: $y = 0.026x + 0.026$. The amount of BHQ3 conjugated on FRT was calculated according to the standard curve: $y = 0.004x + 0.044$.

Characterization of Hybrid Ferritins. The loading efficiencies of ZnPc to ferritin was determined using the UV−vis-NIR spectrometer by measuring absorbance of free ZnPc. Free ZnPc was dissolved in DMSO at different concentrations (0.2, 0.4, 0.6, 0.8, and 1.0 mg/mL), and absorbance was measured by a UV−vis-NIR spectrometer. The amount of loaded ZnPc in hybrid ferritin was calculated according to the standard curve ($y = 3.351x + 0.3$). Fluorescence intensity of the hybrid ferritins were measured by a fluorescence spectrophotometer. To optimize the FABP composition, background fluorescent signals from different ratios of FRT-C3 and FRT-BHQ3 groups were measured and recorded. The fluorescent signals decreased folds were calculated. The size distribution and the zeta potential of hybrid ferritins was measured by dynamic light scattering. The morphology of FABP/ZnPc was observed by transmission electron microscopy (TEM).

Fluorescent Recovery of Hybrid Ferritin. FRT-C3 and FRT-BHQ3 were mixed at pH of 2.0 for 30 min, then the pH was adjusted to 7.4 with 1 M NaOH. After the protein cage was reassembled, caspase-3 of different concentration (2 nM, 5 nM, 10 nM) was added to the solution and incubated in reaction buffer (50 mM HEPES, 100 mM NaCl, 10 mM DTT, 0.1% CHAPS, 10% glycerol, pH = 7.4). For control groups, caspase-3 inhibitor was added to FABP 10 min before caspase-3 was added. The fluorescence activity change of the hybrid ferritin was measured in a cuvette with excitation and emission wavelengths at 675 and 695 nm, respectively, by a fluorescence spectrophotometer. A linear relationship was found between caspases-3 concentration and FABP. The stabilty of FABP/ZnPc in different solutions was investigated.

Detection of Reactive Oxygen Species (ROS). The human breast cancer cell line MDA-MB-435 and mouse embryonic fibroblast cell line NIH3T3 were cultured in DMEM medium containing 10% fetal bovine serum and 1% penicillinstreptomycin at 37 °C with 5% CO_2. MDA-MB-435 cells (1×10^5 cells/well) were seeded on 96-well plates and incubated in complete medium for 24 h at 37 °C. The medium was then replaced with fresh culture medium containing FABP/ZnPc and free ZnPc at different concentrations (20, 10, 5, 2, and 1 μg/mL) and incubated for 4 h at 37 °C. Then, fresh culture medium containing 10 μM DCFH-DA was added and incubated for another 20 min. After washing three times, they were irradiated with a 630 nm laser at a power of 150 mW/cm^2 for 3 min. The fluorescence of DCF was detected with the fluorescence microplate reader with 488 nm excitation and 525 nm emission.

Cell Viability Assays. The cell viability assays was performed by a standard MTT assay. MDA-MB-435 cells (1×10^4 cells/well) and NIH3T3 cells (1×10^4 cells/well) was seeded on 96-well plates and incubated for 24 h at 37 °C. The cells were treated with ZnPc and FABP/ZnPc at different concentrations (50, 25, 12.5, 6.25, and 3 μg/mL) and incubated for 4 h at 37 °C. After incubation, the cells were washed twice with serum-free medium and irradiated with a 630 nm laser at 150 mW/cm^2 for 3 min. In another group, the cells were washed twice with serum-free medium and without irradiation to verify the cell viability in dark conditions. After 6 h incubation, cell viability with irradiation and without irradiation was evaluated by the MTT assay.

Calcein AM and propidium iodide (PI) costaining was also conducted for cell viability assay. Briefly, MDA-MB-435 cells (1×10^5 cells/well) were seeded on six-well plates and incubated for 24 h at 37 °C. Cell culture media were replaced by fresh culture media containing 25 μg/mL FABP/ZnPc. After incubated for 4 h, cells were irradiated by a 630 nm laser (150 mW/cm^2) for 3 min and then washed with PBS three times. After incubation for another 6 h, the cells were stained with calcein AM and PI, which indicate live and dead cells. Afterward, the cells were imaged by fluorescence microscopy.

Cellular Uptake Assay. MDA-MB-435 cells were cultured in DMEM medium containing 10% fetal bovine serum and 1% penicillin-

DOI: 10.1021/acsami.5b07316
ACS Appl. Mater. Interfaces 2015, 7, 23248−23256

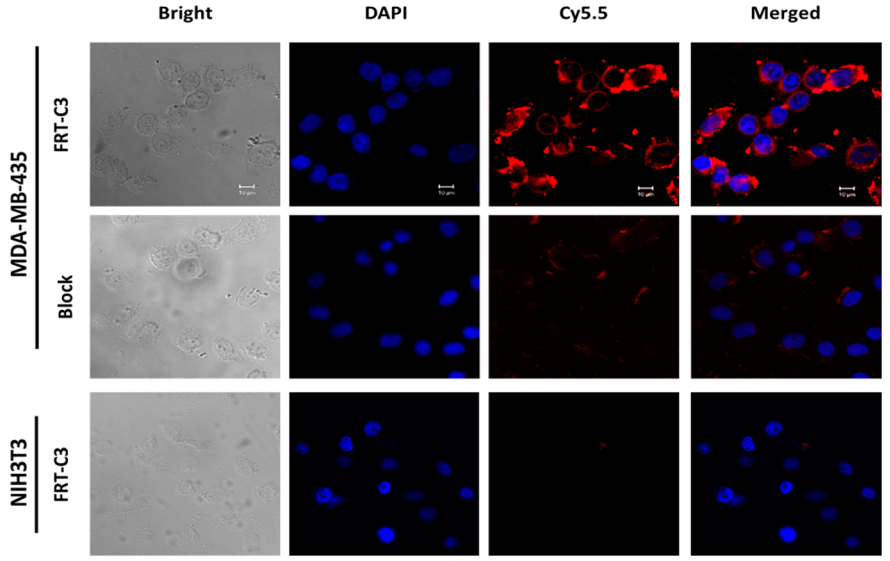

Figure 3. Cell uptake of FRT-C3. MDA-MB-435 cells and NIH3T3 cells were incubated with FRT-C3 for 4 h and then fixed and imaged by confocal microscopy. Free FRT was added 30 min before FRT-C3 to saturate the receptors on the cell membrane.

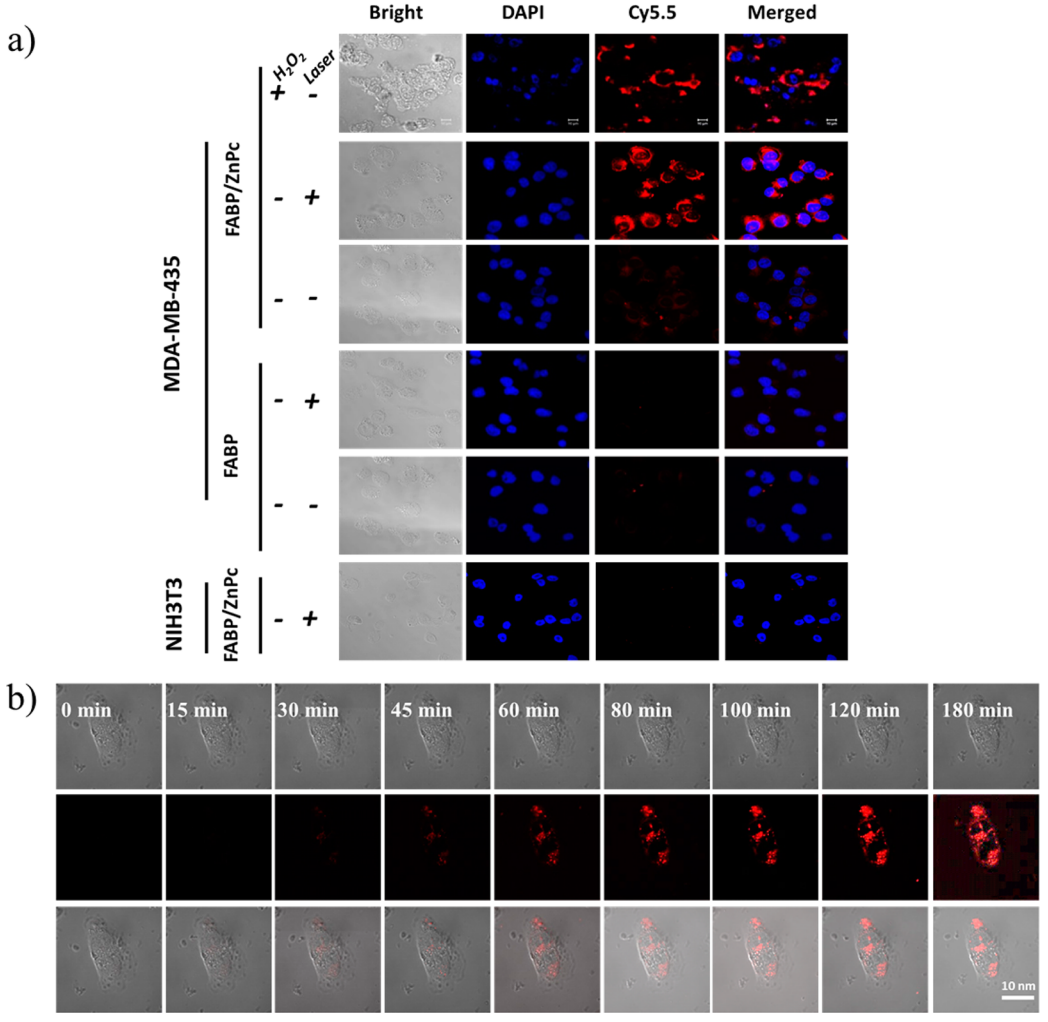

Figure 4. Visualization of caspase-3 activation in MDA-MB-435 cells during PDT. (a) Confocal images of MDA-MB-435 cells and NIH3T3 cells incubated with FABP/ZnPc and FABP in the absence and presence of laser and hydrogen peroxide. (b) Real-time visualization of caspase-3 activation in MDA-MB-435 cells during PDT. The cells were incubated with FABP/ZnPc (containing 0.15 μM of FRT-C3) for 4 h and then treated with 630 nm laser (150 mW/cm^2, 3 min). Images were collected at different time points after laser irradiation over 3 h by confocal laser scanning microscopy.

DOI: 10.1021/acsami.5b07316
ACS Appl. Mater. Interfaces 2015, 7, 23248−23256

streptomycin at 37 °C in a CO_2 incubator. MDA-MB-435 cells (3×10^4 cells/well) were seeded onto an eight-chamber slide and incubated in complete medium for 24 h at 37 °C. FRT-C3 were added to the solution and incubated for 4 h, respectively. After washing with PBS (pH = 7.4) three times, cells were fixed in cold ethanol at −20 °C for 15 min. Then, the slides were mounted with DAPI and imaged by a laser scanning confocal fluorescence microscope (Leica, German).

***In Vivo* NIRF Imaging and PDT Studies.** Animal experiments were conducted under protocols approved by the Animal Care and Use Committee (CCACUCC) of Xiamen University. The MDA-MB-435 animal tumor models were prepared by subcutaneous injection of 5×10^6 cells in l00 μL of PBS into the right shoulder of nude mice. NIRF imaging studies were performed when tumors reached a size approximate to 80 mm^3. We intratumorally (i.t.) injected FABP/ZnPc (1.0 mg ZnPc/kg) in 50 μL of PBS and irradiated by a 630 nm laser for 20 min (150 mW/cm^2). Then, NIRF images was captured at time point of 0.5, 1, 2, 4, 6, and 12 h after laser irradiation (n = 5). Three control groups in different conditions were also performed for NIRF imaging: (1) FABP/ZnPc (1.0 mg ZnPc/kg), without irradiation; (2) FABP, with irradiation; and (3) FABP, without irradiation.

PDT studies were performed when tumors reached a size approximately to 80 mm^3. MDA-MB-435 tumor-bearing mice were randomly divided into 5 groups (n = 5 per/group): (1) FABP/ZnPc (1.0 mg ZnPc/kg), with (w/) 630 nm laser irradiation (150 mW/cm^2, 20 min); (2) FABP/ZnPc (1.0 mg ZnPc/kg), without (w/o) irradiation; (3) FABP, with 630 nm laser irradiation (150 mW/cm^2, 20 min); (4) FABP, without irradiation; (5) untreated. All the nanocomplexes were injected once and the laser irradiations were performed once for treatment. The size of tumors was measured by a digital caliper every other day and the tumor volume was calculated as vol = $ab^2/2$ (a is the longer diameter and b is the shorter diameter). The body weights of all mice were measured every other day.

Statistical Analysis. Results were presented as the mean ± SD. Statistical analysis was performed using one-way ANOVA followed by the Bonferroni multiple comparison test. $P < 0.05$ was considered statistically significant.

RESULTS AND DISCUSSION

Preparation, Optimization, and Characterization of FABP/ZnPc. To develop the probe that can treat cancer and also assess its own therapeutic outcome, we first chemically conjugated a FRET pair before attaching it to FRT and then exploited the FRT assemble/disassemble property to load a metal photosensitizer (ZnPc) inside its self-assembled cage. Specifically, the caspase-3 specific peptide substrate (NH_2-Gly-Asp-Glu-Val-Asp-Ala-Pro-Cys-OH) was synthesized, labeled with a highly fluorescent NIR dye, Cy5.5 (ex/em, 675/695 nm), and named C3 (Figures S1−S3). A difunctional linker, *N*-succinimidyl-4-maleimidobutyrate, was purposely conjugated onto FRT before coupling C3 onto it via thiol-maleimide reaction. The final product was purified by a disposal NAP-5 column and named FRT-C3. Black hole quencher-3 (BHQ3) was also conjugated onto another batch of FRT (FRT-BHQ3) and purified (Figures S2 and S3). After that, the two sets of modified FRT were mixed, and the pH was adjusted to 2.0, conditions that cause each FRT to disassemble into subunits (Figure 1a). After changing the pH back to neutral, a FRT-C3/FRT-BHQ3 hybrid FRT (FABP) was constructed. The amount of Cy5.5 or BHQ3 on FRT was calculated according to standard curves shown in Figure S4. Intact FABP holds low fluorescent signals due to the energy transfer between FRT-BHQ3 and FRT-C3. To minimize the fluorescence background and hence increase the sensitivity of FABP, background signals were optimized and evaluated based on different ratios of FRT-C3 and FRT-BHQ3 (2:1, 1:1, 1:3, 1:5, and 1:9, FRT-C3 concentration was fixed at 0.45 μM) as shown in Figure S5.

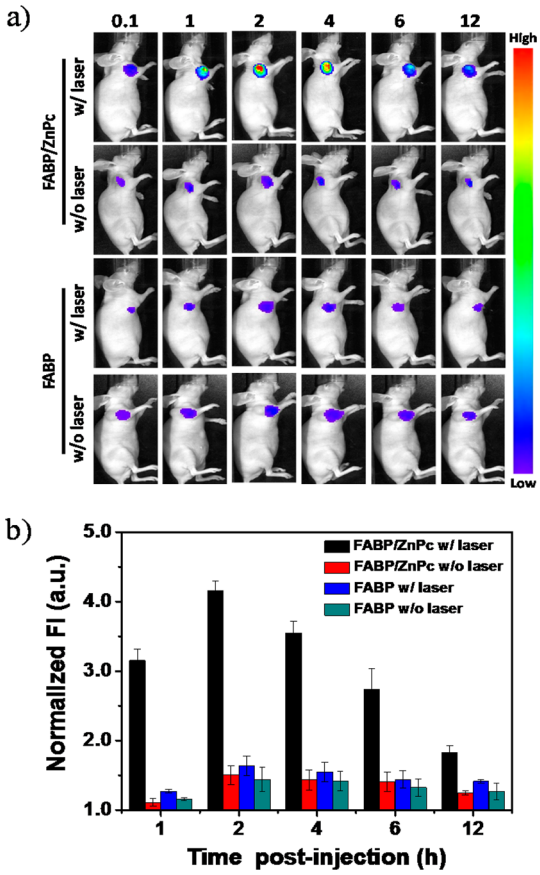

Figure 5. *In vivo* fluorescence imaging of caspase-3 dependent apoptosis during PDT mediated by FABP/ZnPc. MDA-MB-435 tumor-bearing mice were intratumorally administered with FABP/ZnPc (containing 0.45 μM of FRT-C3 and 1.0 mg ZnPc/kg) or FABP (containing 0.45 μM of FRT-C3), respectively. Tumor site was irradiated by a 630 nm laser at 150 mW/cm^2 for 20 min. Then, fluorescent images were acquired 0.5, 1, 2, 4, 6, and 12 h after irradiation for all groups. (a) Caspase-3 activation mediated fluorescent signal increase after PDT over time. (b) Quantification of fluorescent signals in each group after PDT at indicated times.

When the ratio of FRT-C3 to FRT-BHQ3 reached 1:5, a 6.09 ± 0.68 fold decrease in signal was observed. Adding more amount of FRT-BHQ3 did not quench the fluorescent signal any further, suggesting the optimal ratio of FRT-C3/FRT-BHQ3 is 1:5 (Figure S5a,b). Compared with FRT, the size of FABP increased to 14.2 ± 2.68 nm and the zeta potential increased to −4.64 ± 0.63 from −9.07 ± 1.24 due to the labeling of C3 and BHQ3 (Figure S5c).

In order to endow FABP with therapeutic properties, we encapsulated a metal-chelated photosensitizer, zinc(II) phthalocyanine (ZnPc), into FABP by disassembly/reassembly of FRT,[14,15] forming the theranostic nanocomplex FABP/ZnPc (Figure 2a, inserted). Optimizations of ZnPc encapsulated into FABP were listed as in Table S1. Detailed loading and characterization methods are described in Supporting Information (Figures S3 and S6 and Table S1). The size of FABP/ZnPc (15.16 ± 1.2 nm) is about 1 nm larger than FABP alone due to the encapsulated ZnPc, while the zeta potential of FABP/ZnPc (−4.66 ± 1.46) did not change significantly (Figure S5c). Successful construction of FABP/ZnPc was also confirmed by its UV−vis-NIR spectrum. As shown in Figure 2a, characterized peaks of Cy5.5 and BHQ3 in FRT-C3 (red line) and FRT-

DOI: 10.1021/acsami.5b07316
ACS Appl. Mater. Interfaces 2015, 7, 23248−23256

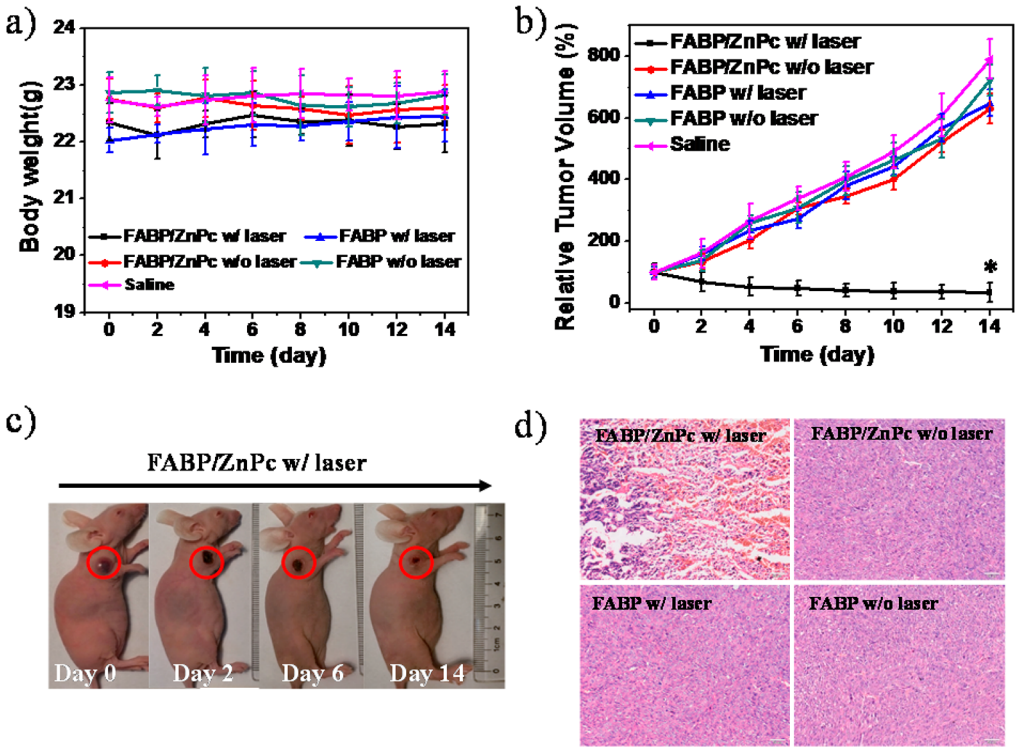

Figure 6. *In vivo* photodynamic therapy (PDT). (a) Body weight curves of MDA-MB-435 tumor-bearing mice for each group. (b) MDA-MB-435 tumor growth rate in each groups after indicated treatments. Tumor volumes were normalized to their initial size (n = 5 per group). For therapeutic groups, mice were intratumoral received with FABP/ZnPc and subjected to 630 nm laser irradiation (150 mW/cm^2, 20 min). Four groups of mice were set as controls: saline group, FABP group with and without laser irradiation, and FABP/ZnPc group without laser irradiation. Error bars were based on standard error of mean (SEM). (c) Representative photos of mice after different treatments. (d) H&E stained tumor sections collected from different groups of mice. Severely damaged tumor tissue was observed in FABP/ZnPc group with laser irradiation. No noticeable abnormality was found in the rest of the groups.

BHQ3 (blue line) were measured, and a blue shift induced by BHQ3 was found after constructing of FRT-C3 and FRT-BHQ3 together (FABP) through pH adjustment. Compared to FABP absorbance spectrum (pink line), a shoulder at around 750 nm was found in the FABP/ZnPc phantom (tan line), which is caused by the encapsulation of ZnPc (aqua line), indicating the successfully loading of ZnPc into FABP. TEM images suggest a globular morphology of FABP/ZnPc with an average size around 15 nm (Figure 2a, inserted). Additionally, the fluorescent signals of FRT-C3 were not affected after encapsulation of ZnPc (Figure S7).

To access the sensitivity of FABP to caspase-3, we incubated 100 nM of FABP with capses-3 (10 nM) in a reaction buffer (50 mM HEPES, 100 mM NaCl, 10 mM DTT, 0.1% CHAPS, 10% glycerol, pH = 7.4) and monitored fluorescent signals over time. As shown in Figure 2b, the original quenched FABP had a low fluorescent signal due to the incompleted quenching effect of BHQ-3 to Cy5.5; but over time, the signal gradually increased and reached a peak after 40 min when the active caspase-3 cleaved its substrate found on the FRT. The cleaved substrate increases the distance between the FRET pairs found on the hybrid FRT and causes reduced quenching effects. As expected, no signal increase was observed in the absence of caspase-3. Moreover, the fluorescent signal was significantly inhibited when caspase-3 inhibitor was treated to the test group (Figure 2c). FABP also showed a linear relationship between the fluorescence intensity and caspase-3 concentration (r^2 > 0.95), indicating that the fluorescence recovery is caspase-3 dependent (Figure S8). Because the goal is to apply FABP/ZnPc for PDT, we examined the fluorescence intensity and stability of FABP/ZnPc under irradiation of a 630 nm laser. The fluorescence of FABP/ZnPc did not change when subjected to laser irradiation for 10 min at a power of 150 mW/cm^2 (Figure 2d). The photostability of FABP/ZnPc was also confirmed by monitoring the morphology and size of FABP/ZnPcby both TEM and DLS. No obvious changes were found after laser irradiation (10 min, 150 mW/cm^2) as shown in Figure S9. FABP/ZnPc was found to be stable in H_2O, PBS, DMEM, and FBS. No obvious NIR-UV−vis absorbance spectra changes of FABP/ZnPc in PBS were found with time, suggesting its potential for applications in physiological environments (Figure S10).

***In Vitro* Photodynamic Toxicity of FABP/ZnPc.** We next evaluated the cytotoxicity of FABP/ZnPc to MDA-MB-435 cells. First, the ROS generation property of FABP/ZnPc was confirmed and quantified by a ROS assay kit containing 2′,7′-dichlorodihydrofluorescin diacetate (DCFH-DA, Beyotime, China), which can be deacetylated by intracellular esterase into 2′,7′-dichlorodihydrofluorescin (DCFH).[41] DCFH can be rapidly oxidized to the highly fluorescent form (ex/em, 488/525 nm) by ROS and the fluorescent intensity is proportional to the ROS levels generated. As shown in Figure S11, FABP/ZnPc demonstrated a similar ROS amount to that of free ZnPc, indicating that the encapsulation does not affect ZnPc properties, which was reported elsewhere as well.[14] According to the UV−vis-NIR spectrum of BHQ-3 and ZnPc, the main absorbance of BHQ-3 is around 600 nm and the peak for ZnPc is around 750 nm. The gap between BHQ-3 and ZnPc

DOI: 10.1021/acsami.5b07316
ACS Appl. Mater. Interfaces 2015, 7, 23248−23256

absorbance may reduce the effect of BHQ-3 on ZnPc generation of ROS. In addition, the typical distance between donor and acceptor is usually in the range of 1−10 nm for fluorescence resonance energy transfer (FRET), while the diameter of the ferritin nanocage is about 15 nm. The relative long distance between BHQ-3 and ZnPc could be another factor that keeps the ZnPc property. The MTT assay and Calcein AM/PI staining revealed that FABP/ZnPc is nontoxic at concentrations up to 50 μg/mL to both MDA-MB-435 and NIH3T3 cells without laser irradiation; however, FABP/ZnPc can cause MDA-MB-435 cancer cell death effectively (IC_{50} = 10 μg/mL) under 630 nm laser irradiation at a power density of 150 mW/cm^2 for 3 min (Figure S12).

***In Vitro* Visualization of Caspase-3 Activation during Apoptosis Induced by PDT.** Because caspase-3 is an intracellular proteinase, FABP/ZnPc must penetrate the cell membrane to the cytoplasm for caspase-3 targeting. It is reported that FRT can bind to certain cell surface receptors, for example, transferrin receptor 1 (TfR1) that is overexpressed in most malignant tumor cell lines compared to the normal cell lines[42−44] and undergoes endocytosis to deliver iron inside cells.[42,45,46] To test this, the cell penetration ability of FABP/ZnPc was investigated by incubating FRT-C3 (Cy5.5, ex/em, 675/695 nm) with MDA-MB-435 cells and NIH3T3 cells. After 4 h incubation, FRT-C3 were found mostly in the cytoplasm of cells, where the caspase cascades activation will take place, without affecting cell morphology (Figure 3). Moreover, excess free ferritin was added to MDA-MB-435 cells 30 min prior to FRT-C3 to block the TfR1. As expected, FRT-C3 was not internalized into negative cells and the block groups. These *in vitro* data illustrate that FABP is a nontoxic nanocarrier with effective cell permeability for intracellular caspase-3 targeting.

The potential of FABP/ZnPc to image caspase-3 activation during PDT in MDA-MB-435 cells was evaluated by confocal microscopy. PDT has been reported to induce cancer cell apoptosis through the activation of the caspase cascade pathway.[34,35,47,48] Apoptosis was validated in MDA-MB-435 cells subjected to PDT by detecting strong fluorescein isothiocyanate labeled Annexin V (FITC-Annexin V) signals on the cells. Similarly, strong FITC-Annexin V signals were found on cells treated with H_2O_2, a known substance to induce apoptosis. In both cases, FITC-Annexin V labeling could be effectively inhibited when excess amounts of free Annexin V were treated to the cells. Specific caspase-3 expression was evaluated by Western blot. Low expression levels of activated caspase-3 were detected in cells without PDT, while more prominent levels of caspase-3 were found after PDT (Figure S13), confirming that PDT can effectively induce apoptosis of MDA-MB-435 cells via a caspase-mediated pathway.

We then used FABP/ZnPc (0.45 μM of FRT-C3) to image caspase-3 activity during PDT in MDA-MB-435 cells and NIH3T3 cells. After incubation, free FABP/ZnPC was washed off and the cells were subjected to 630 nm laser irradiation at 150 mW/cm^2. FABP/ZnPc-treated cells without laser irradiation were used as a control. In addition, FABP was investigated in cells with or without laser irradiation to verify the specificity of FABP/ZnPc to caspase-3. All cells were fixed 2 h after laser irradiation and observed under confocal microscopy. As shown in Figure 4a, strong fluorescent signals were observed in the cytoplasm of cells treated with FABP/ZnPc after laser irradiation, indicating caspase-3 mediated apoptosis. A similar distribution was observed in cells treated with FABP/ZnPc and H_2O_2. However, minimal fluorescent signals were observed in the FABP/ZnPc treated group without laser irradiation. In the absence of ZnPc, where no ROS/$^1O_2$ is generated, no obvious fluorescent signals were found in the cells, suggesting that the fluorescent signal recovery is apoptosis dependent.

To further evaluate the feasibility of FABP/ZnPc on apoptosis imaging, caspase-3 activation was observed in real-time in single live cells (Figure 4b). Cells were treated with FABP/ZnPc as described above. Immediately after laser treatment (150 mW/cm^2, 3 min), cell images were taken by confocal microscopy at 15 min intervals for up to 3 h. A gradually increasing signal was recorded in the cell cytoplasm from 45 min after laser irradiation due to the degradation of FABP/ZnPc by caspase-3. Taken together, these results demonstrate that FABP/ZnPc is capable of real-time imaging of apoptosis at the single cell level and has great potential for targeted imaging of apoptosis *in vivo*.

***In Vivo* Monitoring Caspase-3 Activation during Photodynamic Treatment of Tumor.** Finally, the *in vivo* evaluation of FABP/ZnPc was performed on an MDA-MB-435 tumor bearing mouse model. Tumor cells were inoculated subcutaneously on right flanks. After about 3 weeks when the tumor size reached 80 mm^3, a total of 1.0 mg of ZnPc/kg FABP/ZnPc was injected intratumorally and imaged at different time points (0.5, 1, 2, 4, 6, and 12 h) post laser irradiation. As shown in Figure 5, the FABP/ZnPc administrated group after PDT (150 mW/cm^2, 20 min) demonstrated increased signals in the tumor area over time and reached a peak at 2 h postinjection. Because of blood circulation and metabolism, FABP/ZnPc is slowly washed out of the tumor after 2 h. FABP itself is stable in physiological conditions for 24 has shown in Figure S10. No obvious fluorescent signals were detected due to the lack of caspase-3 activation for the groups treated with FABP/ZnPc or FABP without PDT treatment. The tumor ablation efficiency was confirmed by further monitoring and recording of the tumor growth rate in each group for 14 days (Figure 6 and Figure S14). Compared to the control groups, tumors in the FABP/ZnPc treated group were ablated significantly after laser irradiation, while no obvious body weight changes were found for each.

To further confirm the FABP/ZnPc-mediated photodynamic therapy (PDT) effect, we harvested the tumor tissues treated with FABP and FABP/ZnPc with and without NIR irradiation. The pathological changes of tumors were observed and analyzed by hematoxylin-eosin staining (H&E staining), in which cell nuclei were stained dark blue by positively charged hematoxylin and proteins or amino acids in cytoplasm were stained pink or red by eosin. Compared with control groups, the FABP/ZnPc administrated group clearly showed tumor necrosis and destroyed blood vessels after laser irradiation treatment (Figure 6d), suggesting that FABP/ZnPc effectively destroys tumor tissue with laser irradiation via PDT. No obvious destruction in the tumor was found in FABP/ZnPc groups without laser irradiation.

CONCLUSION

PDT has been considered as an alternative approach for many diseases. Monitoring apoptosis induced by PDT plays an important role in predicting and improving the outcome of the treatment.[49] Thus, development of effective, sensitive, and biocompatible imaging agents would be of great benefit for current treatment strategies. In this study, we successfully

DOI: 10.1021/acsami.5b07316
ACS Appl. Mater. Interfaces 2015, 7, 23248−23256

engineered ferritin nanocages that can effectively and simultaneously induce PDT of tumors and image PDT-induced apoptosis *in vitro* and *in vivo*. By tuning the ratio of dye/quencher labeled FRTs, we were able to optimize the composition of a hybrid FRT with effective sensitivity and specificity to caspases-3. The feasibility of such a hybrid ferritin nanocomplex for caspase-3 imaging during PDT was confirmed in living cells as well as a tumor bearing model. Overall, the FABP/ZnPc holds the advantages of high biostability, photostability, improved sensitivity, and great promise for *in vitro* and *in vivo* applications over the previous reported probes. We anticipate that this strategy will offer new opportunity for understanding of the mechanisms of PDT-induced apoptosis and also be helpful for screening and evaluating the therapeutic potential for a broad of new photosensitizers. A metal-chelated photosensitizer was trapped in FABP in this study; alternatively, the other kinds of photosensitizers can also be loaded into FABP by harnessing the disassemble/self-assemble property of FRT for therapy purposes. On the other hand, the engineered ferritin platform can be extended to target other proteinase or multiple targets at same time for more practical applications, for example, investigation of caspases cascade activation during PDT or photothermal therapy (PTT). Practically, clinical approved photosensitizers can be loaded into the FABP complex modified with targeted moieties for *in vivo* effective PDT, providing the potential of translating the ferritin theranostic system into the clinic.

■ ASSOCIATED CONTENT

Supporting Information

The Supporting Information is available free of charge on the ACS Publications website at DOI: 10.1021/acsami.5b07316.

Probe fabrication, morphology, and environmental stability, TEM imaging and cell viability, FABP enzyme activity test, ROS generation, Annexin V staining, Western blot, cell uptake, and *in vivo* experiments (PDF)

■ AUTHOR INFORMATION

Corresponding Authors

*Phone: (+)86-592-2880642. Fax: (+)86-592-2880642. E-mail: lei.zhu@xmu.edu.cn.

*E-mail: gaoshi800830@163.com.

Author Contributions

The manuscript was written through contributions of all authors. All authors have given approval to the final version of the manuscript.

Notes

The authors declare no competing financial interest.

■ ACKNOWLEDGMENTS

This work was supported by National Science Foundation of China (NSFC) (Grants 81201129, 51373144, and 81501506), National High Technology Research and Development Program of China (863 Program) (Grant No. 2014AA020708), Fundamental Research Funds for the Central Universities (Grant No. 20720150064), Science Foundation of Xiamen City (Grant No. 3502Z20140045), and the Science Foundation of Fujian Province (Grant No. 2014Y2004).

■ REFERENCES

(1) Sokolovski, G.; Goltsov, A.; Pourreyron, C.; South, P.; Rafailov, U. Infrared Laser Pulse Triggers Increased Singlet Oxygen Production in Tumour Cells. *Sci. Rep.* **2013**, *3*, 3484.

(2) Dolmans, E.; Fukumura, D.; Jain, K. Photodynamic Therapy for Cancer. *Nat. Rev. Cancer* **2003**, *3*, 380−387.

(3) Celli, J. P.; Spring, B. Q.; Rizvi, I.; Evans, C. L.; Samkoe, K. S.; Verma, S.; Pogue, B. W.; Hasan, T. Imaging and Photodynamic Therapy: Mechanisms, Monitoring, and Optimization. *Chem. Rev.* **2010**, *110*, 2795−2838.

(4) Elich, D.; Lagarias, C. Phytochrome Chromophore Biosynthesis: Both 5-Aminolevulinic Acid and Biliverdin Overcome Inhibition by Gabaculine in Etiolated Avena Sativa L. *Plant Physiol.* **1987**, *84*, 304−310.

(5) Tanaka, M.; Kataoka, H.; Yano, S.; Ohi, H.; Moriwaki, K.; Akashi, H.; Taguchi, T.; Hayashi, N.; Hamano, S.; Mori, Y.; Kubota, E.; Tanida, S.; Joh, T. Antitumor Effects in Gastrointestinal Stromal Tumors Using Photodynamic Therapy with a Novel Glucose-Conjugated Chlorin. *Mol. Cancer Ther.* **2014**, *13*, 767−775.

(6) Rizvi, I.; Anbil, S.; Alagic, N.; Celli, J.; Zheng, L. Z.; Palanisami, A.; Glidden, D.; Pogue, W.; Hasan, T. Pdt Dose Parameters Impact Tumoricidal Durability and Cell Death Pathways in a 3D Ovarian Cancer Model. *Photochem. Photobiol.* **2013**, *89*, 942−952.

(7) Fan, Y.; Bergmann, A. Apoptosis-Induced Compensatory Proliferation. The Cell Is Dead. Long Live the Cell. *Trends Cell Biol.* **2008**, *18*, 467−473.

(8) Zheng, X.; Wang, X.; Mao, H.; Wu, W.; Liu, B.; Jiang, X. Hypoxia-Specific Ultrasensitive Detection of Tumours and Cancer Cells in Vivo. *Nat. Commun.* **2015**, *6*, 5834.

(9) Casas, A.; Di Venosa, G.; Hasan, T. Mechanisms of Resistance to Photodynamic Therapy. *Curr. Med. Chem.* **2011**, *18*, 2486−2515.

(10) Vickers, J.; Gonzalez-Paez, E.; Wolan, W. Discovery of a Highly Selective Caspase-3 Substrate for Imaging Live Cells. *ACS Chem. Biol.* **2014**, *9*, 2199−2203.

(11) Wang, L.; Chen, T.; Qu, J.; Wei, X. Quantitative Analysis of Caspase-3 Activation by Fitting Fluorescence Emission Spectra in Living Cells. *Micron* **2009**, *40*, 811−820.

(12) Zhu, L.; Huang, X.; Choi, Y.; Ma, Y.; Zhang, F.; Liu, G.; Lee, S.; Chen, X. Real-Time Monitoring of Caspase Cascade Activation in Living Cells. *J. Controlled Release* **2012**, *163*, 55−62.

(13) Kalluru, P.; Vankayala, R.; Chiang, C. S.; Hwang, K. C. Photosensitization of Singlet Oxygen and in Vivo Photodynamic Therapeutic Effects Mediated by Pegylated W(18)O(49) Nanowires. *Angew. Chem., Int. Ed.* **2013**, *52*, 12332−12336.

(14) Zhen, Z.; Tang, W.; Guo, C.; Chen, H.; Lin, X.; Liu, G.; Fei, B.; Chen, X.; Xu, B.; Xie, J. Ferritin Nanocages to Encapsulate and Deliver Photosensitizers for Efficient Photodynamic Therapy against Cancer. *ACS Nano* **2013**, *7*, 6988−6996.

(15) Zhen, Z.; Tang, W.; Chuang, J.; Todd, T.; Zhang, W.; Lin, X.; Niu, G.; Liu, G.; Wang, L.; Pan, Z.; Chen, X.; Xie, J. Tumor Vasculature Targeted Photodynamic Therapy for Enhanced Delivery of Nanoparticles. *ACS Nano* **2014**, *8*, 6004−6013.

(16) Ge, J.; Lan, M.; Zhou, B.; Liu, W.; Guo, L.; Wang, H.; Jia, Q.; Niu, G.; Huang, X.; Zhou, H.; Meng, X.; Wang, P.; Lee, S.; Zhang, W.; Han, X. A Graphene Quantum Dot Photodynamic Therapy Agent with High Singlet Oxygen Generation. *Nat. Commun.* **2014**, *5*, 4596.

(17) Niu, G.; Chen, X. Apoptosis Imaging: Beyond Annexin V. *J. Nucl. Med.* **2010**, *51*, 1659−1662.

(18) Fan, T. J.; Han, H.; Cong, S.; Liang, J. Caspase Family Proteases and Apoptosis. *Acta Biochim. Biophys. Sin.* **2005**, *37*, 719−727.

(19) McIlwain, R.; Berger, T.; Mak, W. Caspase Functions in Cell Death and Disease. *Cold Spring Harbor Perspect. Biol.* **2013**, *5*, a008656.

(20) Chang, Y.; Yang, L. Proteases for Cell Suicide: Functions and Regulation of Caspases. *Microbiol Mol. Biol. Rev.* **2000**, *64*, 821−846.

(21) Courtiade, J.; Pauchet, Y.; Vogel, H.; Heckel, D. G. A Comprehensive Characterization of the Caspase Gene Family in Insects from the Order Lepidoptera. *BMC Genomics* **2011**, *12*, 357.

DOI: 10.1021/acsami.5b07316
ACS Appl. Mater. Interfaces 2015, 7, 23248−23256

(22) Perez-Hernandez, M.; Del Pino, P.; Mitchell, G.; Moros, M.; Stepien, G.; Pelaz, B.; Parak, J.; Galvez, M.; Pardo, J.; de la Fuente, M. Dissecting the Molecular Mechanism of Apoptosis During Photothermal Therapy Using Gold Nanoprisms. *ACS Nano* **2015**, *9*, 52−61.
(23) Louie, A. Multimodality Imaging Probes: Design and Challenges. *Chem. Rev.* **2010**, *110*, 3146−3195.
(24) Min, Y.; Li, J.; Liu, F.; Yeow, K.; Xing, B. Near-Infrared Light-Mediated Photoactivation of a Platinum Antitumor Prodrug and Simultaneous Cellular Apoptosis Imaging by Upconversion-Luminescent Nanoparticles. *Angew. Chem., Int. Ed.* **2014**, *53*, 1012−1016.
(25) Huang, X.; Lee, S.; Chen, X. Design of "Smart" Probes for Optical Imaging of Apoptosis. *Am. J. Nucl. Med. Mol. Imaging* **2011**, *1*, 3−17.
(26) Barnett, M.; Zhang, X.; Maxwell, D.; Chang, Q.; Piwnica-Worms, D. Single-Cell Imaging of Retinal Ganglion Cell Apoptosis with a Cell-Penetrating, Activatable Peptide Probe in an in Vivo Glaucoma Model. *Proc. Natl. Acad. Sci. U. S. A.* **2009**, *106*, 9391−9396.
(27) Zhu, L.; Zhang, F.; Ma, Y.; Liu, G.; Kim, K.; Fang, X.; Lee, S.; Chen, X. In Vivo Optical Imaging of Membrane-Type Matrix Metalloproteinase (MT-MMP) Activity. *Mol. Pharmaceutics* **2011**, *8*, 2331−2338.
(28) Zhang, L.; Gao, S.; Zhang, F.; Yang, K.; Ma, Q.; Zhu, L. Activatable Hyaluronic Acid Nanoparticle as a Theranostic Agent for Optical/Photoacoustic Image-Guided Photothermal Therapy. *ACS Nano* **2014**, *8*, 12250−12258.
(29) Huang, X.; Swierczewska, M.; Choi, Y.; Zhu, L.; Bhirde, A.; Park, J.; Kim, K.; Xie, J.; Niu, G.; Lee, C.; Lee, S.; Chen, X. Multiplex Imaging of an Intracellular Proteolytic Cascade by Using a Broad-Spectrum Nanoquencher. *Angew. Chem., Int. Ed.* **2012**, *51*, 1625−1630.
(30) Ye, D.; Shuhendler, J.; Cui, L.; Tong, L.; Tee, S.; Tikhomirov, G.; Felsher, W.; Rao, J. Bioorthogonal Cyclization-Mediated in Situ Self-Assembly of Small-Molecule Probes for Imaging Caspase Activity in Vivo. *Nat. Chem.* **2014**, *6*, 519−526.
(31) Shah, K.; Tang, Y.; Breakefield, X.; Weissleder, R. Real-Time Imaging of Trail-Induced Apoptosis of Glioma Tumors in Vivo. *Oncogene* **2003**, *22*, 6865−6872.
(32) Niu, G.; Zhu, L.; Ho, N.; Zhang, F.; Gao, H.; Quan, Q.; Hida, N.; Ozawa, T.; Liu, G.; Chen, X. Longitudinal Bioluminescence Imaging of the Dynamics of Doxorubicin Induced Apoptosis. *Theranostics* **2013**, *3*, 190−200.
(33) Laxman, B.; Hall, E.; Bhojani, S.; Hamstra, A.; Chenevert, L.; Ross, D.; Rehemtulla, A. Noninvasive Real-Time Imaging of Apoptosis. *Proc. Natl. Acad. Sci. U. S. A.* **2002**, *99*, 16551−16555.
(34) Wu, Y.; Xing, D.; Chen, W. R. Single Cell Fret Imaging for Determination of Pathway of Tumor Cell Apoptosis Induced by Photofrin-PDT. *Cell Cycle* **2006**, *5*, 729−734.
(35) Stefflova, K.; Chen, J.; Li, H.; Zheng, G. Targeted Photodynamic Therapy Agent with a Built-in Apoptosis Sensor for in Vivo near-Infrared Imaging of Tumor Apoptosis Triggered by Its Photosensitization in Situ. *Mol. Imaging* **2006**, *5*, 520−532.
(36) Lovell, J. F.; Chan, W.; Qi, Q.; Chen, J.; Zheng, G. Porphyrin Fret Acceptors for Apoptosis Induction and Monitoring. *J. Am. Chem. Soc.* **2011**, *133*, 18580−18582.
(37) Stefflova, K.; Chen, J.; Zheng, G. Killer Beacons for Combined Cancer Imaging and Therapy. *Curr. Med. Chem.* **2007**, *14*, 2110−2125.
(38) Yogo, T.; Urano, Y.; Ishitsuka, Y.; Maniwa, F.; Nagano, T. Highly Efficient and Photostable Photosensitizer Based on Bodipy Chromophore. *J. Am. Chem. Soc.* **2005**, *127*, 12162−12163.
(39) Uzdensky, B.; Iani, V.; Ma, L. W.; Moan, J. Photobleaching of Hypericin Bound to Human Serum Albumin, Cultured Adenocarcinoma Cells and Nude Mice Skin. *Photochem. Photobiol.* **2002**, *76*, 320−328.
(40) Lin, X.; Xie, J.; Zhu, L.; Lee, S.; Niu, G.; Ma, Y.; Kim, K.; Chen, X. Hybrid Ferritin Nanoparticles as Activatable Probes for Tumor Imaging. *Angew. Chem., Int. Ed.* **2011**, *50*, 1569−1572.
(41) Tian, J.; Ding, L.; Xu, H. J.; Shen, Z.; Ju, H.; Jia, L.; Bao, L.; Yu, J. S. Cell-Specific and Ph-Activatable Rubyrin-Loaded Nanoparticles for Highly Selective near-Infrared Photodynamic Therapy against Cancer. *J. Am. Chem. Soc.* **2013**, *135*, 18850−18858.
(42) O'Donnell, K. A.; Yu, D.; Zeller, K. I.; Kim, J. W.; Racke, F.; Thomas-Tikhonenko, A.; Dang, C. V. Activation of Transferrin Receptor 1 by C-Myc Enhances Cellular Proliferation and Tumorigenesis. *Mol. Cell. Biol.* **2006**, *26*, 2373−2386.
(43) Gatter, C.; Brown, G.; Trowbridge, S.; Woolston, E.; Mason, D. Y. Transferrin Receptors in Human Tissues: Their Distribution and Possible Clinical Relevance. *J. Clin. Pathol.* **1983**, *36*, 539−545.
(44) Niitsu, Y.; Kohgo, Y.; Nishisato, T.; Kondo, H.; Kato, J.; Urushizaki, Y.; Urushizaki, I. Transferrin Receptors in Human Cancerous Tissues Tohoku. *Tohoku J. Exp. Med.* **1987**, *153*, 239−243.
(45) Liang, M.; Fan, K.; Zhou, M.; Duan, D.; Zheng, J.; Yang, D.; Feng, J.; Yan, X. H-Ferritin-Nanocaged Doxorubicin Nanoparticles Specifically Target and Kill Tumors with a Single-Dose Injection. *Proc. Natl. Acad. Sci. U. S. A.* **2014**, *111*, 14900−14905.
(46) Gatter, K. C.; Brown, G.; Trowbridge, I. S.; Woolston, R. E.; Mason, D. Y. Transferrin Receptors in Human Tissues: Their Distribution and Possible Clinical Relevance. *J. Clin. Pathol.* **1983**, *36*, 539−545.
(47) Stefflova, K.; Chen, J.; Marotta, D.; Li, H.; Zheng, G. Photodynamic Therapy Agent with a Built-in Apoptosis Sensor for Evaluating Its Own Therapeutic Outcome in Situ. *J. Med. Chem.* **2006**, *49*, 3850−3856.
(48) Chen, J.; Stefflova, K.; Niedre, J.; Wilson, C.; Chance, B.; Glickson, D.; Zheng, G. Protease-Triggered Photosensitizing Beacon Based on Singlet Oxygen Quenching and Activation. *J. Am. Chem. Soc.* **2004**, *126*, 11450−11451.
(49) Lee, S.; Mortensen, J.; Lin, P.; Tung, C. An Authentic Imaging Probe to Track Cell Fate from Beginning to End. *Nat. Commun.* **2014**, *5*, 5216.

DOI: 10.1021/acsami.5b07316
ACS Appl. Mater. Interfaces 2015, 7, 23248−23256